

3. Results

3. 1. Analysis of *c-Jun* and *JunD* expression in bone cells and bone tumors

The aim of this work was to define the function of *c-Jun* and *JunD* in bone development and to determine their influence in osteosarcoma and osteosclerosis formation in mutated mice over-expressing *c-Fos* or *Fra-1*. Therefore, I first investigated *c-Jun* and *JunD* expression in bone and tumor cells cultured *in vitro*. For this purpose I analyzed their expression on RNA level by RT-PCR and on protein level by Western blotting of nuclear extracts from primary osteoblasts or tumor cells, isolated from wild type, *fra-1* tg and *c-fos* tg mice.

c-Jun and *JunD* mRNA were both found to be expressed in wild type, *fra-1* tg and *c-fos* tg primary bone cells (figure 3.01). The proteins were also detected in nuclear extract isolated from the various cells (figure 3.02).

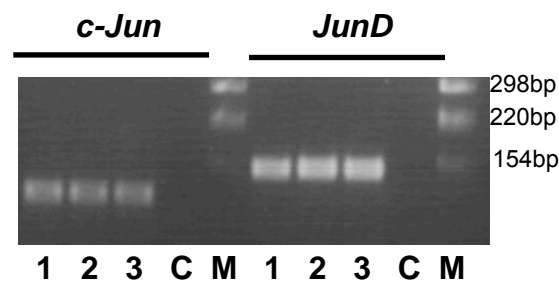


Figure 3.01. Expression of *c-Jun* and *JunD* transcripts in primary bone cells. mRNA from *wild type* (1), *fra-1* tg (2) primary osteoblasts and *c-fos* tg (3) primary tumor cells were isolated, digested with DNaseI, subjected to cDNA synthesis and subsequently amplified by PCR. As control, one reaction without cDNA (C) was run. Amplification products were separated on a 2 % w/v agarose gel.

Since *JunD*-RNA harbors an alternative translation initiation site, two isoforms of *JunD* are synthesized and recognized by the *JunD*-antibody. The additional band appearing in the western blot for *JunD* are non specific cross-reactivities.

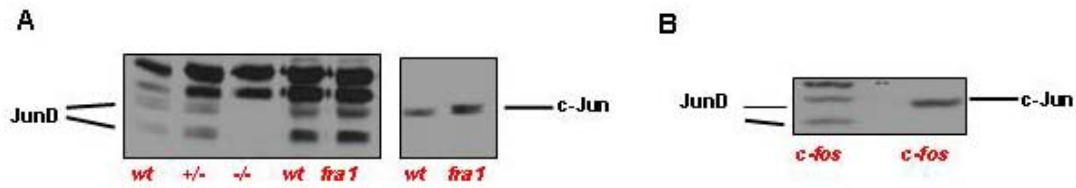


Figure 3.02. Expression of c-Jun and JunD in primary bone cells. Nuclear extracts from primary osteoblasts (A) or primary tumour cells (B) with the indicated genotype (highlighted in red) were separated by SDS-PAGE, transferred on nitrocellulose and incubated with JunD and c-Jun antibodies.

In vivo, c-Jun and JunD expression were analyzed in tumor developing in *c-fos* tg mice by immunofluorescence, both were found to be expressed (figure 3.03).

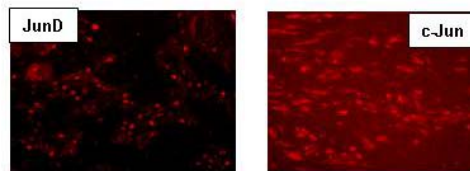


Figure 3.03. c-Jun and JunD are expressed in osteosarcoma. Paraffin sections were deparaffinized, boiled in citrate buffer and incubated with c-Jun and JunD antibodies. After incubation with secondary antibody coupled to rhodamine red, c-Jun and JunD expression in tumour sections could be observed by fluorescence microscopy.

3. 2. *c-Jun* function in bone development

3. 2. 1. Conditional deletion of *c-jun* by crossing *c-jun*^{fl/fl} mice with Runx2-cre mice

Since the lack of *c-jun* leads to embryonic lethality, the study of c-Jun functions in bone biology needed to be performed by a conditional approach. To delete *c-jun* in bone tissue, I choose a mouse strain expressing Cre under the control of a bone specific promoter: The promoter of Runx2, a transcription factor expressed in hypertrophic chondrocytes and in early osteoblast was chosen. This mouse strain

was demonstrated to specifically and efficiently delete two different floxed genes in bone tissue (J. Tuckermann, personal communication).

After crossing *Runx2-cre* mice with *c-jun^{fl/fl}* mice, I isolated different tissues from double mutant offsprings and performed genotyping by PCR for the deletion of *c-jun* using primers specifically amplifying the recombinant *c-jun* allele. The deletion was not detected in samples prepared from bone of endochondral (long bone) or in bone from intra-membranous origin (calvaria). In addition, no amplification was obtained in cartilage tissue samples such as sternum and ribs. As expected there was no deletion observed in the bone marrow sample since the *Runx2* promoter is not active in haematopoietic and uncommitted stromal cells. The deletion of *c-jun* could only be detected in DNA samples isolated from the growth plate. Even though deletion took place in the growth plate, the efficiency was very low since the intensity of the band representing the floxed allele was not altered in comparison to samples obtained from mice only harboring the floxed allele and not expressing Cre. In addition the band resulting from the recombination event was very weak (figure 3.04). Therefore the analysis of c-Jun function in bone development and its contribution to c-Fos induced osteosarcoma or Fra-1-induced osteosclerosis was not possible *in vivo* using *Runx2* promoter-mediated Cre expression.

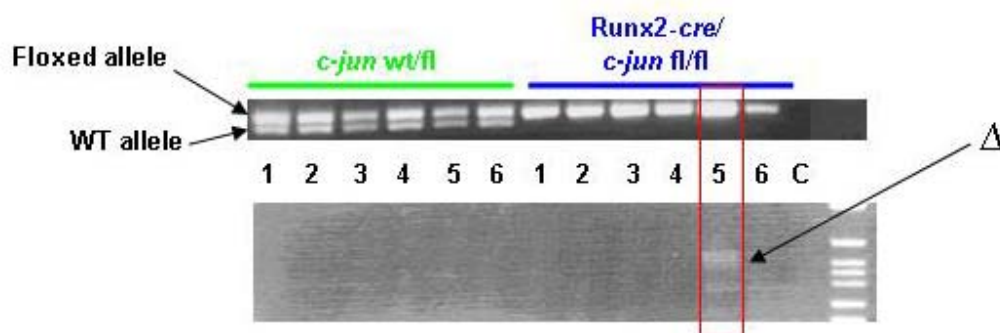


Figure 3.04. *c-jun* is not efficiently deleted in bone by *Runx2-cre*. The samples deriving from *c-jun^{wt/fl}* mice without *Runx2-cre* allele (highlighted by green bar) do not display recombination events in any tissue analyzed. Samples from mice harboring *Runx2-cre* and floxed *c-jun* allele (blue bar) show only the bands resulting from *c-jun* recombination in tissue originating from the growth plate (lane 5, indicated by red rectangle) even though efficiency is very low (Δ band on lower panel). Lane 1: long bone (without bone marrow), lane 2: calvaria, lane 3: ribs, lane 4: sternum, lane 5: growth plate, lane 6: bone marrow, lane C: control (no template)

3. 2. 2. Conditional deletion of *c-jun* in *in vitro* cultures of primary osteoblasts by means of infection with Cre-encoding virus

Because the deletion efficiency was very low and in the absence of any other suitable bone specific Cre-mouse strain in the laboratory, I decided to analyze the function of c-Jun in osteoblasts by inducing its deletion *in vitro*. Therefore, I isolated primary osteoblasts from *c-jun*^{wt/wt}, *c-jun*^{wt/fl} and *c-jun*^{fl/fl} mice and infected them with viral supernatants containing *cre*-coding sequences (MSCV-Cre). After selecting stably infected osteoblasts, I prepared nuclear extracts to check for the level of c-Jun expression in the various infected cells.

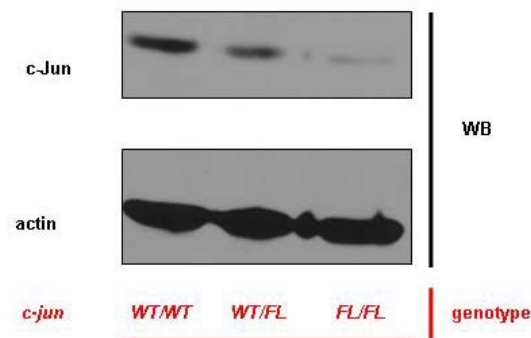


Figure 3.05. Expression of c-Jun is strongly decreased in *c-jun*^{fl/fl} primary osteoblasts infected with Cre-encoding virus. Following infection, nuclear extracts of primary osteoblasts with the indicated genotypes (red) were separated by SDS-PAGE, transferred on nitrocellulose membrane and incubated with c-Jun antibody (upper panel) and subsequently with β -actin antibody (lower panel) as loading control. A strong reduction is seen in the lane loaded with extracts from *c-jun*^{fl/fl} extracts comparing to extracts from *c-jun*^{wt/wt} cells. An intermediate level of expression is seen in *c-jun*^{wt/fl}.

The expression level of c-Jun was strongly reduced in the infected *c-jun*^{fl/fl} osteoblasts. An intermediate level of c-Jun expression is observed in *wt/fl* infected cells. So deletion of *c-jun* by viral Cre infection was very efficient and dose dependent (figure 3.05). However, following selection, the infected primary cells were undergoing crisis and no cell lines carrying the deletion could be established, therefore the system could not be used for further analyses.

3. 3. *c-Jun* function in *c-Fos* induced tumor formation

3. 3. 1. Conditional deletion of *c-jun* *in vitro* in *c-fos* tg cell lines by means of viral infection, impact of *c-Jun* in cell growth properties

A similar strategy was used to delete *c-Jun* in cell lines established from cells isolated from *c-Fos*-induced osteosarcomas. For studying the impact of *c-Jun* in *c-Fos* induced transformed osteoblasts, I generated a cell line from *c-fos* tg/*c-jun*^{fl/fl} tumors and infected this cell line with Cre-GFP-virus and control (MSCV-GFP) virus. The infected cells were selected by cell sorting and efficiency of deletion was assessed by quantitative RT-PCR and western blot analysis. The levels of *c-Jun* transcript were strongly decreased in cells infected with Cre-GFP virus when compared to cells infected with control plasmid (figure 3.06).

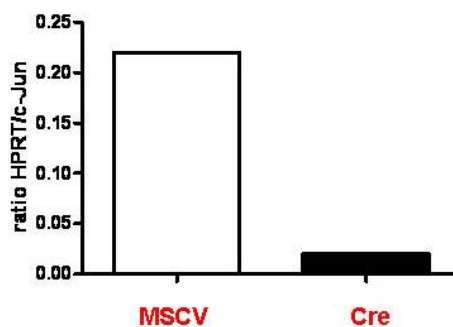


Figure 3.06. The expression of *c-Jun* transcript is strongly decreased in *c-fos* tg/*c-jun*^{fl/fl} transformed osteoblasts infected with Cre-encoding virus. The level of expression was measured by quantitative PCR. *c-Jun* expression levels were normalized to *HPRT* expression. *c-Jun* expression of Cre-infected cells is less than 10 % compared to control cells (MSCV empty vector)

c-Jun protein expression was also drastically reduced in Cre-GFP infected cells but not in cells with control vector (figure 3.07).

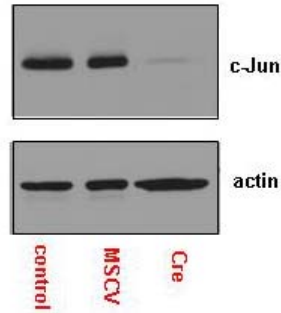


Figure 3.07. c-Jun expression is strongly decreased in Cre infected *c-fos tg/c-jun^{fl/fl}* cells. Western blot analysis of c-Jun expression in nuclear extracts prepared from sorted *c-fos tg/c-jun^{fl/fl}* cell line infected with empty vector (MSCV-GFP) or Cre-GFP. The blot was incubated with c-Jun antibody (upper panel) and subsequently with β -actin antibody as loading control. c-Jun is hardly detectable in cells infected with Cre-GFP (Cre) virus comparing to MSCV-GFP virus infected cells (MSCV) or non-infected cells (control).

These cells were used to analyze the impact of c-Jun deletion on the cell cycle profile by FACS analysis (figure 3.08 and 3.09). The percentage of cells in S-phase was only 7.59 % in *c-fos tg/c-jun^{Δ/Δ}* tumor cell in comparison to 17.09 % in *c-fos tg/c-jun^{fl/fl}* tumor cells. The percentage of cells in G1-phase (73.52 % vs. 79.77 %) is elevated in *c-fos tg/c-jun^{Δ/Δ}* tumor cells while percentage of cells in G2M-phase (9.4 % vs. 12.29 %) was only slightly increased in *c-fos tg/c-jun^{Δ/Δ}* tumor cells. These results suggested that the transition from G1 to S-phase was impaired in Fos transgenic cells lacking c-Jun.

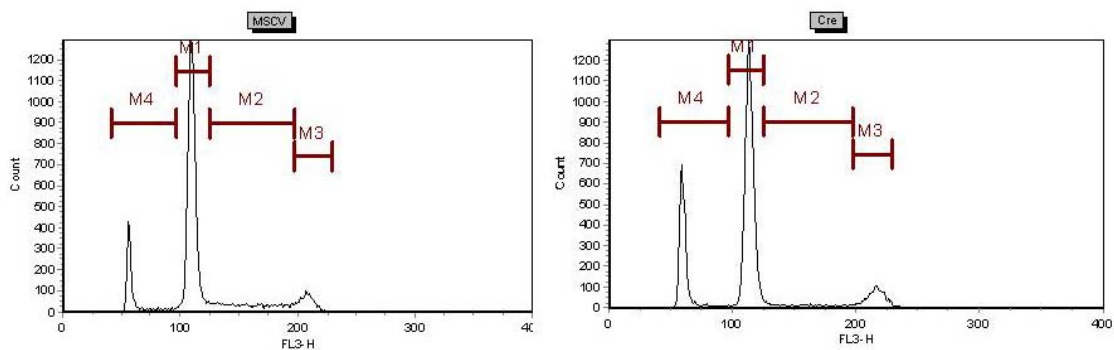


Figure 3.08. Cell cycle profiles of MSCV-GFP (left panel) and Cre-GFP (right panel) infected *c-fos tg/c-jun^{fl/fl}* cell line were analysed by FACS. Brown bars indicate cell cycle phase.

M1: G1-phase, M2: S-phase, M3: G2M-phase, M4: dead cells

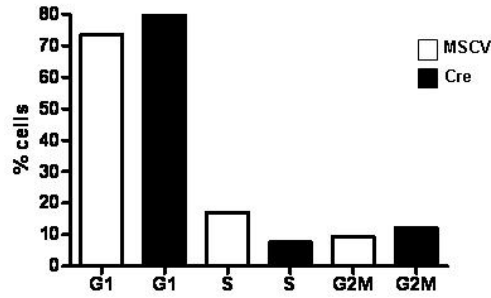


Figure 3.09. Decreased S-phase cell number in Cre infected *c-fos tg/c-jun^{f/f}* cells. The percentage of cells in S-phase was strongly decreased in *c-fos tg/c-jun^{f/f}* cells infected with Cre (black bars) compared to control (white bars). Percentage of G1 and G2M phase were elevated in Cre infected cells.

Another read-out of the FACS analysis was the higher percentage of dead cells (figure 3.10) in *c-fos tg/c-jun^{Δ/Δ}* cells (22.28 % compared to 13.77 %) indicating that c-Jun is required for Fos transgenic cell survival.

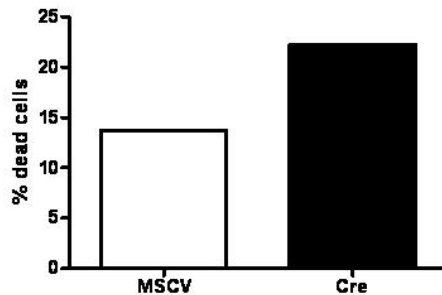


Figure 3.10. Increased cell death in *c-fos tg/c-jun^{f/f}* cells infected with Cre.

After 3 passages of the selected GFP positive cells, the cells were sorted again to exclude non-infected cells which might have escaped the initial sorting procedure. The amount of GFP positive cells were compared to earlier passages. The second sorting revealed a higher proportion of population of GFP negative cells in the tumor cells infected with Cre-GFP encoding virus. The cells infected with MSCV-GFP-control plasmid did only display a small fraction of GFP-negative cells. These results suggest that the c-Fos transgenic cells with a functional c-Jun have a strong advantage in cell propagation compared to the tumor cells lacking c-Jun.

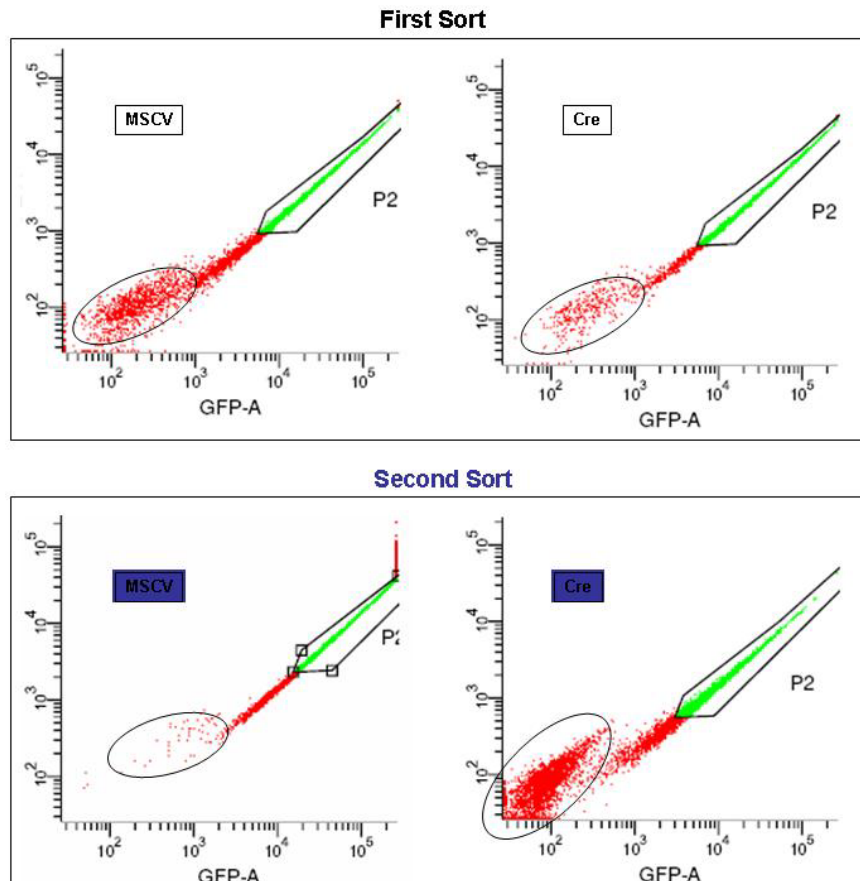


Figure 3.11. Results of first and second cell sorting of *c-fos tg/c-jun^{fl/fl}* cell lines infected with control vector and Cre. The upper panel shows the result of the first sorting. The encircled cell populations are GFP-negative. From the GFP-positive populations only the highly GFP-expressing cells (P2, indicated in green) were selected by sorting for further cultivation. The second sorting (lower panel) reveals a big population of GFP-negative cells only in the Cre-GFP infected cells while the GFP-negative population in MSCV-GFP infected cells was very low. These data suggest that Cre-GFP- positive and as a consequence *c-Jun* lacking cells have a disadvantage in cell growth.

In summary these experiments demonstrate that *c-Jun* is required for cell cycle progression and protects the tumoral cells from cell death thereby putting the cells lacking *c-Jun* under strong selective pressure.

3. 4. *JunD* function in bone development

3. 4. 1. *JunD* function in bone development *in vivo*

The bone of *junD*-deficient mice has, so far, not been analyzed. I bred *junD* heterozygote animals to obtain all genotype constellations and sacrificed them at the age of 4, 12 and 20 weeks in order to analyze several bone parameters. Measuring

the body weight of the animals confirmed previous studies that *junD*^{-/-} animals are slightly growth retarded compared to wild type littermates (figure 3.12).

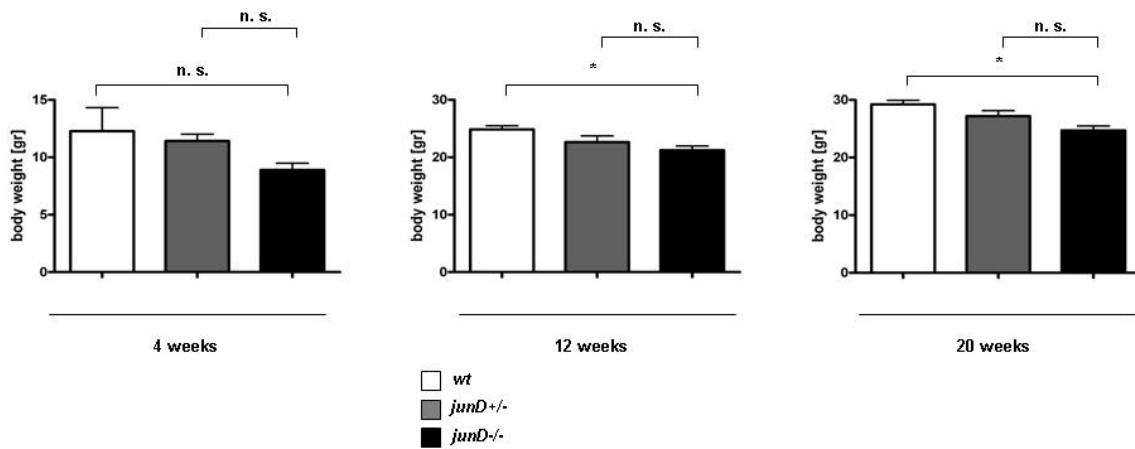


Figure 3.12. Reduced body weight in *junD*^{-/-} male mice.

Osteoblasts, myocytes and adipocytes are originating from a common mesenchymal precursor, thus, defect in osteoblasts differentiation can affect fat and muscular tissues. Therefore, I also measured the weight of spleen, heart and fat pads. The ratio of heart/fat pads to body weight is one read out for potential heart defect. The ratio fat pad/body weight is indicative of the defect that can affect adipogenesis. In addition these data can provide information about general metabolic statute. The ratio spleen/body weight is often increased due to extramedullary haematopoiesis when bone defects cause occlusion of bone marrow space. This is observed when bone resorption is impaired (osteopetrosis) or when bone formation is increased (osteosclerosis). None of these parameters were significantly affected by JunD deletion (figure 3.13).

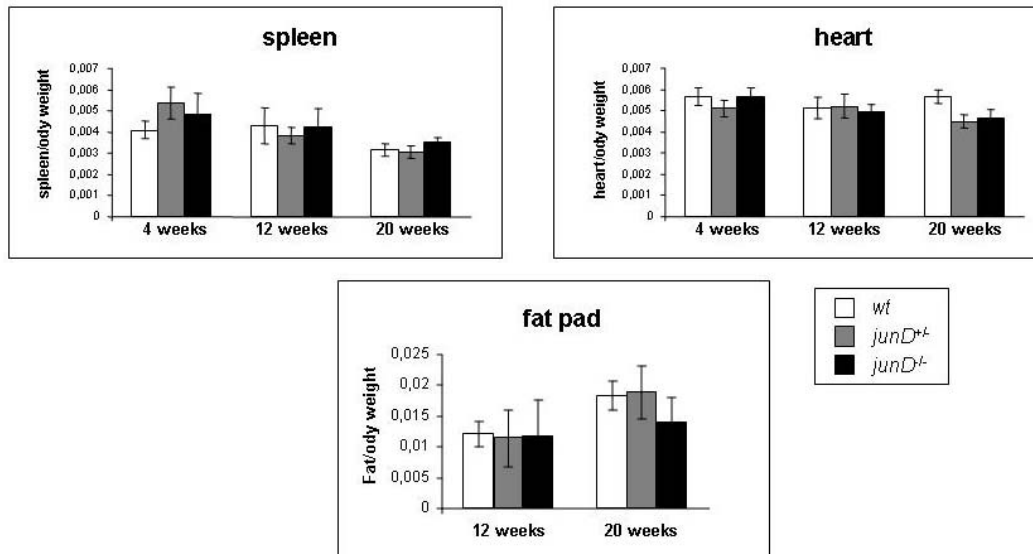


Figure 3.13. Normal spleen-, heart- and fat pad- to body weight ratio in *junD*^{-/-} mice.

I next measured the bone mineral density of the animals (figure C.14). Bone mineral density of male *JunD* deficient mice at 4 and 12 weeks of age were not significantly different from wild type or heterozygote littermates. However at 20 weeks of age bone mineral density was significantly increased in *junD* KO animals. 20 weeks old *junD* KO mice had ~5 % higher bone mass than wild type or heterozygote littermates. While a reduction in the bone mass is observed between of the 12 weeks and 20 weeks in wild type and heterozygote mice, the bone mass appears to be unchanged in the aging *JunD* deficient mice. A conclusion to be drawn from these experiments is that *junD* deficient mice are protected against age induced bone loss.

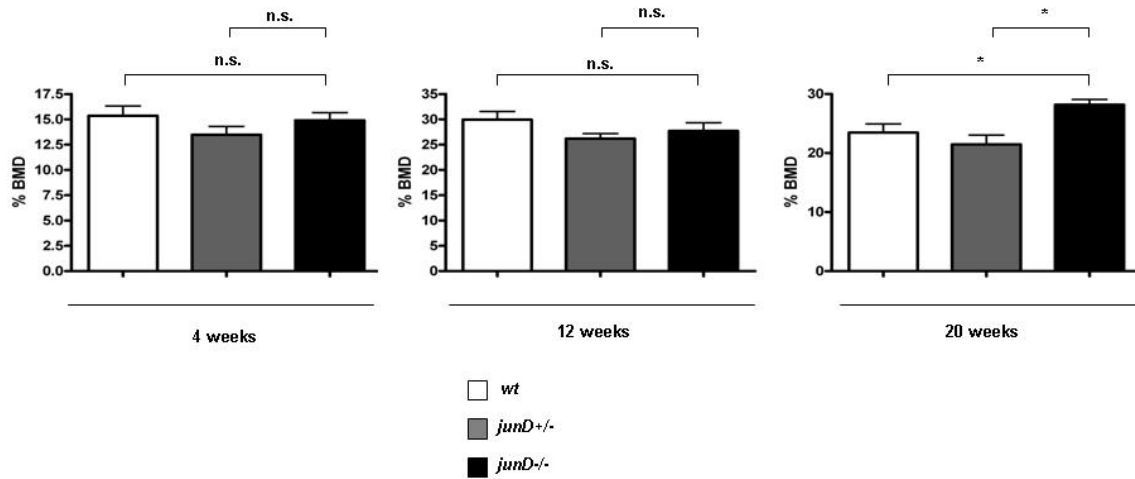


Figure 3.14. Increased bone mineral density in *junD*^{-/-} male mice at 20 weeks of age. There are no significant changes between the genotypes in bone mineral density at 4 and 12 weeks of age. After reaching peak bone mass at 12 weeks of age, the wild type and *junD*^{+/-} animals lost bone mass while *junD*^{-/-} animals were protected against bone loss.

Ovariectomy is an established model to mimic postmenopausal estrogen-deficiency induced bone loss that is commonly observed in aging women. Therefore, I performed ovariectomy on 12 weeks old female wild type and *junD* KO mice. 8 weeks after surgery, animals were sacrificed and bone mineral density was measured on non decalcified section of the bone stained by Von Kossa staining. In Von Kossa staining mineralized areas are stained in black. An increased mineralized area is observed in the ovariectomized *junD* deficient animals compared to wild type. Quantification of bone mineral density revealed a ~50 % higher bone mass in *junD* KO mice compared to *junD* wild type control. Thus mice lacking *junD* are protected against estrogen deficiency induced bone loss.

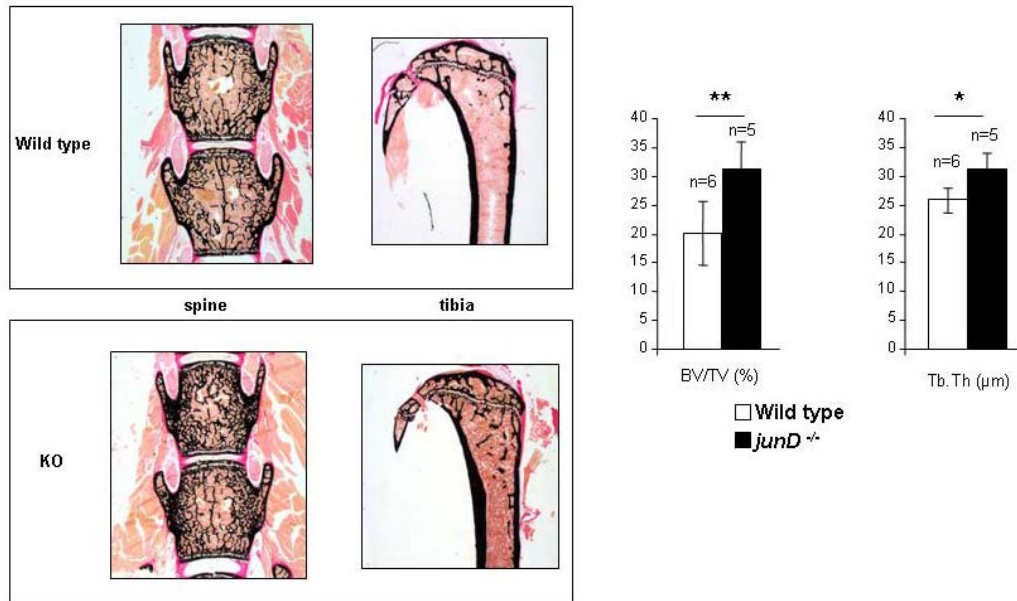


Figure 3.15. *junD*^{-/-} mice are protected against ovariectomy-induced bone loss. 12 weeks old *junD* wild type and *junD*^{-/-} female mice were sacrificed 8 weeks after surgery and bone parameters were determined. The upper panel shows sections from the spine and the tibia of *wild type* mice and the lower panel from *junD* KO mice. The mineralized areas are stained black. Note the larger black areas in the *junD* KO sections. Quantification of bone volume versus tissue volume revealed a highly significant increase in mineralized bone mass in *junD* KO females as well as a significant increase in trabecular thickness.

3. 4. 2. JunD function in primary osteoblasts

To check if the increased bone mass in *junD* KO mice observed *in vivo* is due to a cell autonomous increase of osteoblasts function, I isolated primary osteoblasts from wild type, heterozygous and knock out animals and measured proliferation and apoptosis (figure 3.14). Both of these parameters were similar between the different genotypes.

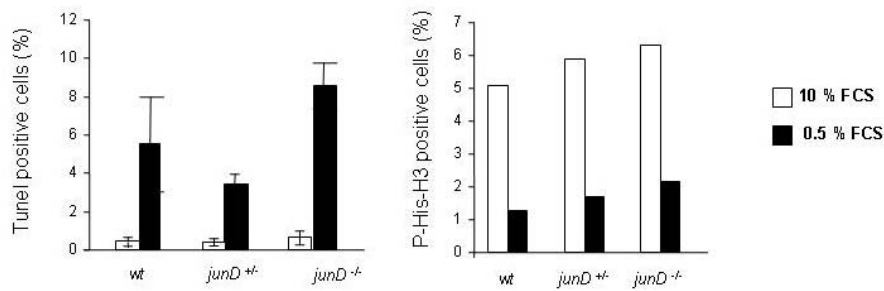


Figure 3.14. Apoptosis and proliferation rate are similar in wild type, *junD*^{+/-} and *junD*^{-/-} primary osteoblasts. Apoptosis was assessed by TUNEL staining (left graph) and proliferation by counting cells positive for the proliferation marker phospho-histone 3 (right graph). The cells originating from the different genotypes displayed a similar response in 10 % FCS culture conditions (white columns) as well as under serum deprivation (black columns). The data are expressed as proportion of positive cells.

I next checked the differentiation capacity of the primary osteoblasts. Cells were cultured in mineralization media for 21 days and stained with alizarine red to revealed matrix mineralization. An increased mineralization of matrix was observed in culture of osteoblasts derived from *junD* KO compared to wild type and heterozygote cells (figure 3.15). Thus, JunD deletion that did not affect cell death and proliferation is resulting in cell autonomous increased osteoblasts differentiation.

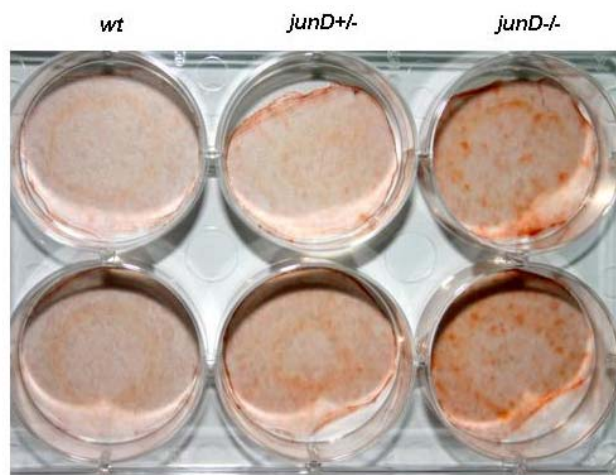


Figure 3.15. Alizarine Red staining of primary osteoblasts. *junD*^{-/-} primary osteoblasts display enhanced differentiation capacity.

3. 5. Impact of JunD in Fra-1 induced osteosclerosis

To assess the role of JunD in osteosclerotic *fra-1* tg mice, I crossed *fra-1* tg mice with *junD* KO mice to obtain *fra-1* tg/*junD* KO double mutants. I did not obtain any viable *fra-1* tg/*junD* KO mutants but all the other genotypic constellations were observed. Few dead pups were found and genotyped as double mutants. This indicated that *fra-1* tg/*junD* KO double mutants were dying during embryonic development or shortly after birth. Therefore I was not able to analyze the participation of JunD in Fra-1 induced osteosclerosis.

3. 6. Role of JunD in c-Fos induced osteosarcoma formation

Over-expression of c-Fos in mice results in osteosarcoma formation with 100 % penetrance. To define the role played by JunD in this process, I crossed *c-fos* tg mice with *junD* deficient mice. Progenies of these crossings were obtained with mendelian frequency (figure 3.16).

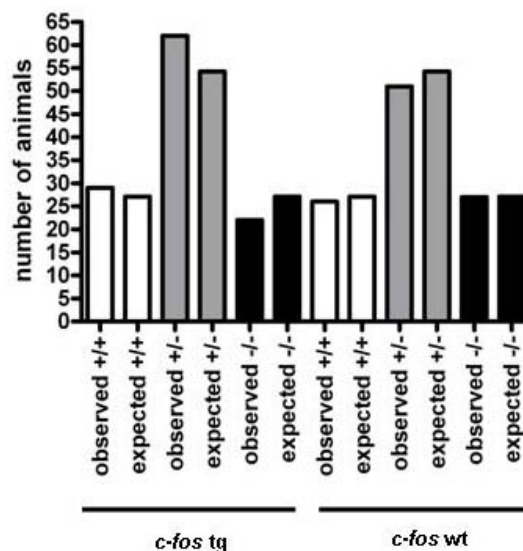


Figure 3.16. Mendelian distribution of genotypes from *c-fos* tg/*junD*^{+/-} male crossed with *junD*^{+/-} female.

Analysis of heart/body weight- and spleen/body weight-ratio did not reveal significant changes between *c-fos-tg/junD* KO and wild type animals (figure 3.17).

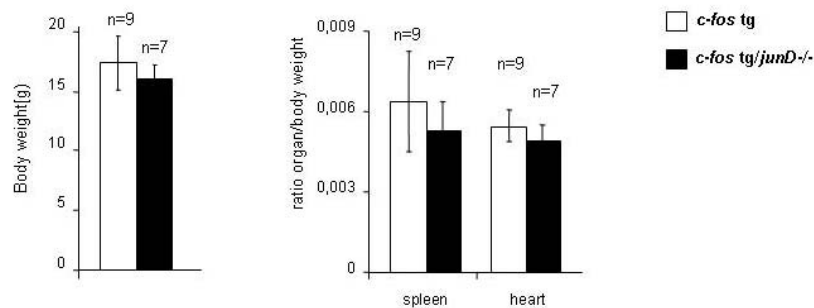


Figure 3.17. No significant change in body weight and in spleen or heart to body weight ratio between *c-fos tg* and *c-fos tg/junD^{-/-}* male 12 week old mice.

At 12 weeks of age, the *c-fos-tg/junD^{-/-}* double mutants appeared healthier in comparison to their *c-fos tg* littermates. The double mutants were not affected in locomotion while the *c-fos tg* animals display already first signs of paralysis most likely due to the progression of the tumors often located on the joints.

When skeletal elements were dissected, the tumors developing in *c-fos tg/junD^{-/-}* mice appeared smaller when compared to *c-fos tg* mice (figure 3.17).

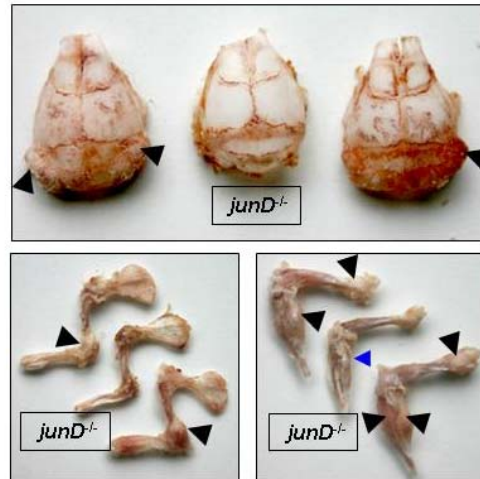


Figure 3.17. Decreased tumor size in skeletal elements of 12 weeks old male *c-fos tg/junD^{-/-}* mice compared to *c-fos tg* mice. Black arrowheads indicate tumors in calvaria (upper panel), upper limbs (lower left panel) and hind limbs (lower right panel). Tumors from *c-fos tg/junD^{-/-}* mice were only visible in the tibia highlighted by a blue arrowhead.

X-ray analysis of the skeletons did confirm the smaller tumor sizes in the double mutants (figure 3.18). Full skeletons were prepared and fixed for detailed histomorphometric analysis and quantitative measurement of tumor size.

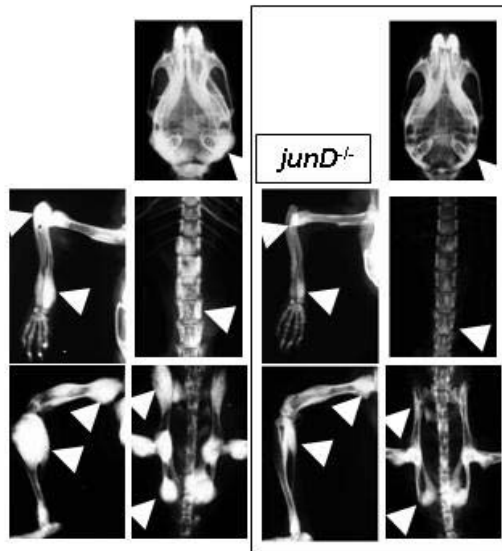


Figure 3.18. X-ray analysis of 12 weeks old male *c-fos* tg and *c-fos* tg/*junD*^{-/-} mice. Radio dense tumors are indicated by white arrowheads. While the location and the frequency of the tumors within the skeleton are comparable tumor size is strongly decreased in *c-fos* tg/*junD*^{-/-} animals (left panel) compared to *c-fos* tg (right panel).

Figure 3.19 shows sections of the spine and the tibia stained by Von Kossa. Again tumor size is strongly reduced in the double mutants (figure 19). Quantification of tumor volume in relation to the whole tissue volume revealed a more than 70 % decrease in the size of tumors developing in *c-fos* tg/*junD*^{-/-} mice compared to *c-fos* tg mice although the incidence of tumor formation is not affected by *junD* deletion (figure 3. 19).

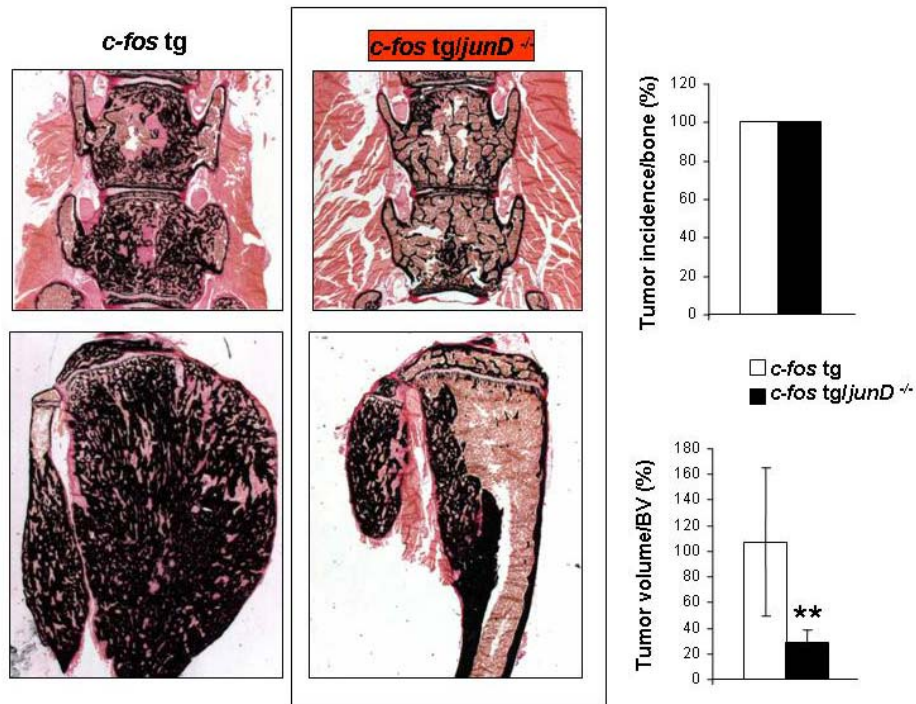


Figure 3.19. Histologic analysis of tumors. Decrease of *c-fos tg/junD^{-/-}* tumor volume in relation to total bone volume can be seen by von Kossa staining and is highly significant. Tumor incidence is unchanged in *c-fos tg/junD^{-/-}* mice.

The data indicated that JunD is essential for c-Fos induced tumor progression but not for tumor initiation.

I next analysed the mineralization content of tumor tissue. The ratio mineralized tumor volume versus tissue volume is significantly reduced in tumors lacking JunD (figure 3.20). This indicates that in addition to its osteosarcoma promoting role, JunD also affects c-Fos induced osteosarcoma by influencing tumor mineralization.

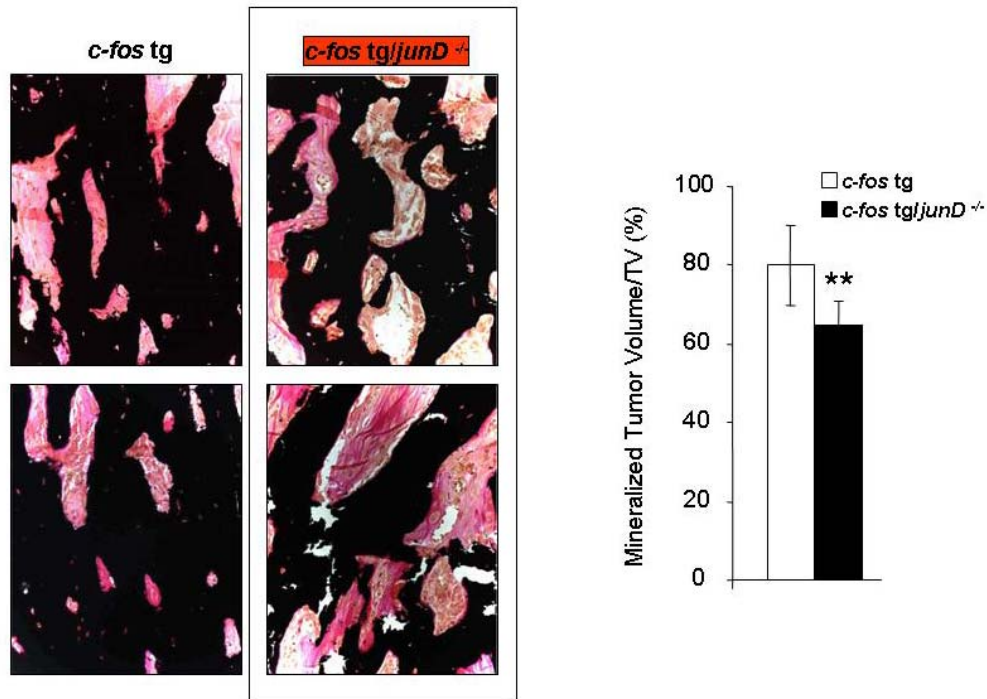


Figure 3.20. Mineralized tumor volume is significantly decreased in *c-fos tg/junD^{-/-}* tumors. Tumor sections were stained by Von Kossa method. Non-mineralized areas (white and pink) are increased in *c-fos tg/junD^{-/-}* tumor sections.

To get insights into the cellular mechanisms which could account for the reduction in tumor size in JunD lacking mice, I generated cell lines from the tumors. I established two cell lines from *c-fos tg/junD^{+/-}* and *c-fos-tg/junD^{-/-}* tumors each. The expression level of AP-1 members was measured by quantitative RT-PCR (figure 3.21) and western blot analysis (figure 3.22). There was no correlation between genotype of the lines and the level of expression of transcripts for AP-1 members with the exception of *JunD* which, as expected, was not expressed in the *c-fos tg/junD^{-/-}* cell lines.

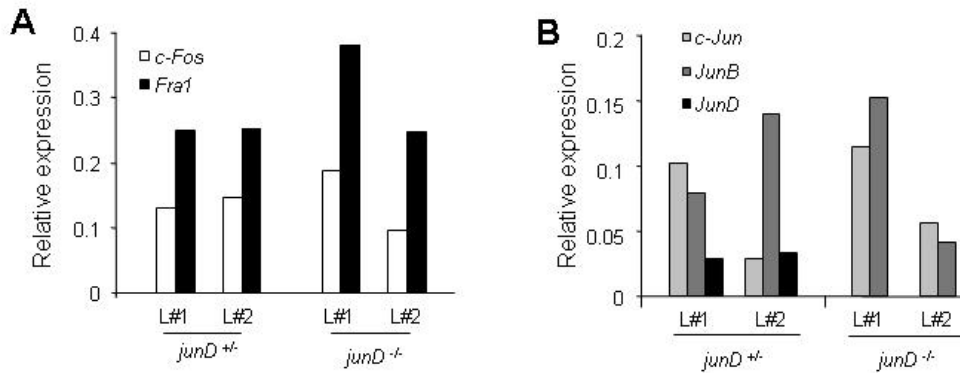


Figure 3.21. mRNA expression analysis of AP-1 members. (A) Expression of *c-Fos* and *Fra-1*. (B) mRNA levels of *c-Jun*, *JunB* and *JunD*. There were no significant changes in expression of the various AP-1 members observed between the two genotype groups except of *JunD* expression which was not detectable in the *c-fos* tg/*junD*^{-/-} cell lines as expected.

At the protein level *c-Fos* and *c-Jun* expression were not affected by the absence of *JunD* (figure 3.22). In addition, I analysed the expression level of the kinase *Rsk2* recently shown by our group to be essential for *c-Fos* induced tumor progression. *RSK2* was not changed (figure 3.22). So the alteration of tumor progression observed in the absence of *JunD* is likely to be independent of *Rsk2*.

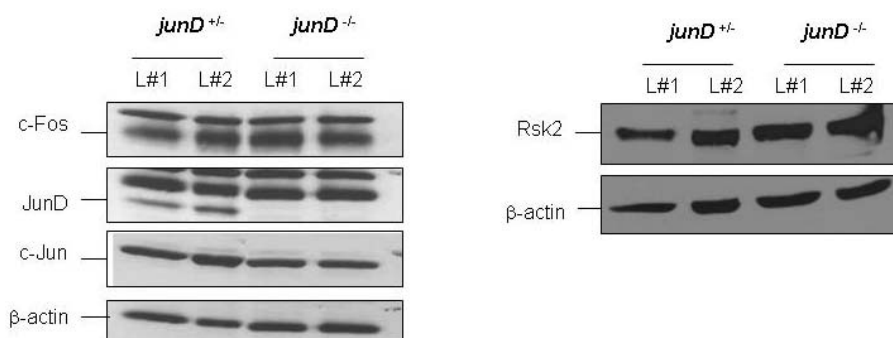


Figure 3.22. Protein expression of AP-1 members and Rsk2. (left panel) Expression of AP-1 member *c-Fos* and *c-Jun* were not altered. *JunD* was not detected in *c-fos* tg/*junD*^{-/-} cell lines. (right panel) Expression of the *c-Fos* kinase *Rsk2* was not altered.

Resistance to apoptosis-induced cell death combined to deregulation of cell cycle control are two characteristics of transformed cells that favored their proliferation. In addition, tumor cells are often getting independent of growth factors for their survival and proliferation. Therefore, I first checked the effect of growth factor deprivation (i.e.

decreased serum concentration) on the growth of the isolated cell lines. An increased sensitivity to serum deprivation was observed with both cell lines lacking JunD (figure 3.23-A). Therefore I further measured proliferation and apoptosis rate of the cells to determine which of these parameters could account for the reduced cell growth observed in low serum conditions. The proliferation rate was similar in all cell lines under normal and low serum conditions (figure 3.23-B). The percentage of apoptotic cells was comparable between the different cell lines cultured in high serum condition. However, under serum deprivation the apoptotic rate was increased ~2 fold in the JunD lacking cell lines (figure 3.23-C-D).

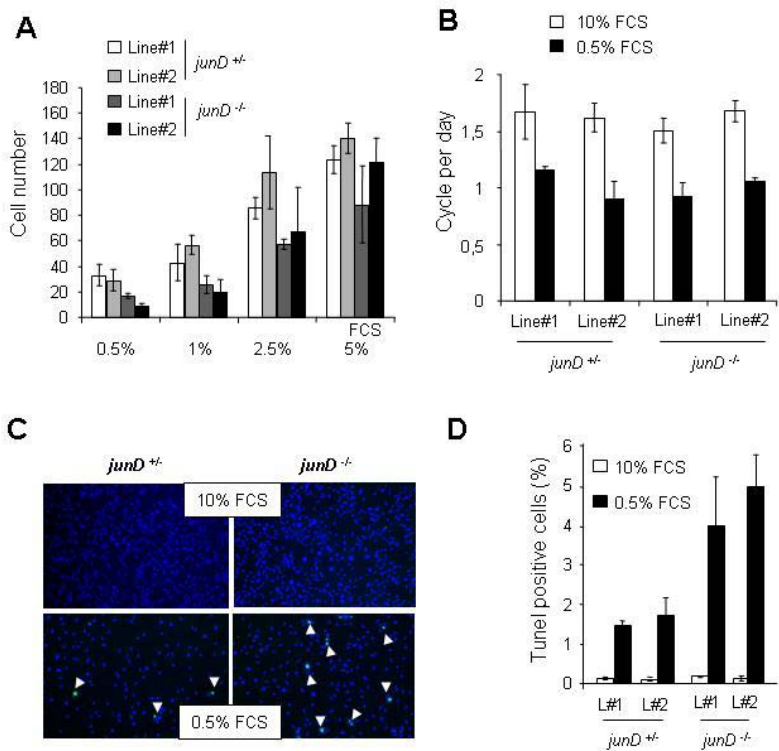


Figure 3.23. Increase in apoptosis rate of *c-fos tg/junD*^{-/-} cell lines under low serum condition. A: cell growth was determined under different serum concentrations. *c-fos tg/junD*^{-/-} cell lines display reduced growth rates in 0.5 %-2.5 % FCS culture conditions. In 5 % FCS media, cell growth is comparable to *c-fos tg/junD*^{+/+} cell lines. B: Reduced cell number in *c-fos tg/junD*^{-/-} cell lines under low serum condition is not due to altered proliferation rates. C: Determination of apoptosis by TUNEL staining. There were more TUNEL positive (apoptotic) cells observed (green) in *c-fos tg/junD*^{-/-} cell lines in 0.5 % FCS than in control cell lines. D: Quantification of TUNEL positive cells reveals a ~2-fold increase of apoptotic cells in *c-fos tg/junD*^{-/-} cell lines in 0.5 % FCS media compared to control.

I next wanted to determine the tumorigenic properties of the isolated cell lines *in vivo*. For this purpose I injected the cell lines into 4-6 weeks old NUDE-mice. 4 weeks after injection, the animals were sacrificed and the tumors arising in the mice analyzed. Tumors which arose from the control cell line were bigger than the ones originating from the JunD deficient cell line (figure 3.24) indicating that JunD promotion of tumor progression is cell autonomous.

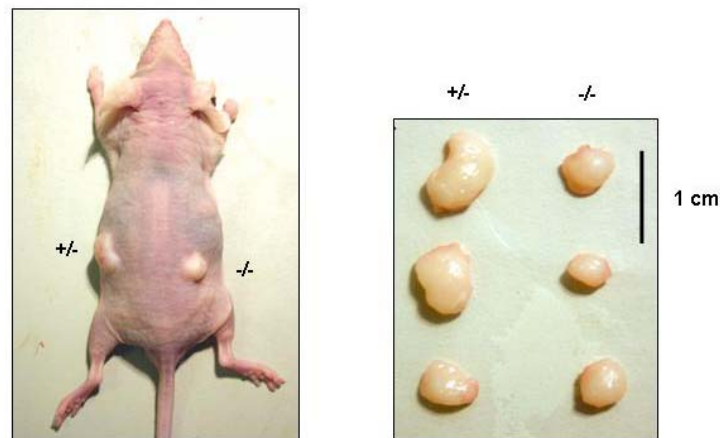


Figure 3.24. Tumors arising from injection of the *c-fos tg/junD^{-/-}* cell lines in Nude mice were smaller than the ones from the *c-fos tg/junD^{+/-}* controls.

3. 6. 1. Expression analysis of genes related to tumor formation, cell cycle progression and apoptosis in tumor samples from *c-fos tg* and *c-fos tg/junD KO* mice

The expression of several genes known to be involved in tumor formation and putative AP-1 targets was measured by quantitative RT-PCR (figure 3.25). First, I determined the expression level of the *fos* transgene which was not significantly changed (figure 3.25). CyclinD1 which is a known c-Fos target gene as well as the master regulator of tumor repression p53 and its downstream target p21 were not differentially expressed. In contrast the cyclin dependant kinase (CDK) inhibitor p27 was increased by ~2 fold in the samples lacking JunD. p8, a gene recently shown to be essential for tumor progression and which I also found strongly up-regulated in a

genomic screen in *c-fos* tg tumor samples (data not shown) was down-regulated in JunD deficient osteosarcoma samples by ~2-fold.

Thus the role of JunD in osteosarcoma progression is not mediated via the p53 pathway or by regulating the transcription of cyclinD1 but may involve positive regulation of the transcriptional co-factor p8 and down regulation of the CDK inhibitor p27.

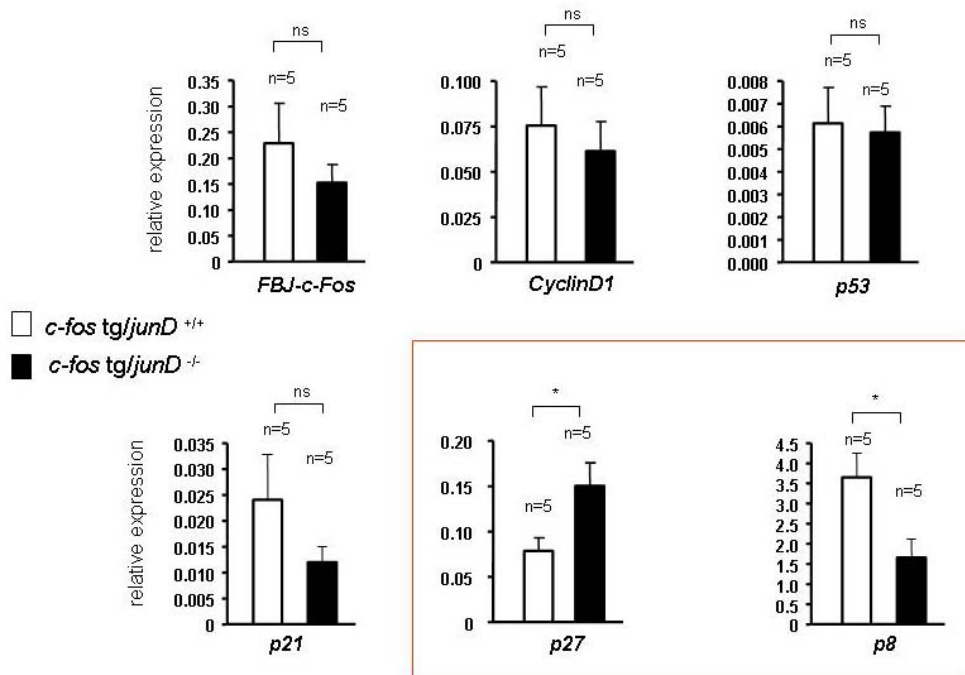


Figure 3.25. mRNA expression level of genes related to cell cycle progression, apoptosis and tumor formation. Expression of the *c-Fos* transgene (*FBJ-c-Fos*), *cyclinD1*, *p53* and *p21* were not significantly changed. In contrast CDK inhibitor *p27* was up-regulated and transcriptional co-factor *p8* was down-regulated in tumors from *c-fos* tg/*junD*^{-/-} mice.

3. 6. 2. Expression analysis of genes related to vascularization and senescence

Vascularization that provides nutritional supply is an important component of solid tumor growth. Interestingly JunD was described as a negative regulator of angiogenesis; thus, I checked the expression of master regulators of vessel formation *Vegfa* and the known *c-Fos* target gene *Vegfδ*. Their expression was not significantly altered by JunD deletion (figure 3.26).

Senescence is a cellular mechanism that can counteract oncogenic stimuli and was identified in several cancer models as an efficient strategy for cells to suppress transformation. In addition, JunD deficient immortalized fibroblasts were reported to undergo premature senescence. I checked the expression level of 2 markers for senescence, Dec1 and p15 that have been involved in negatively controlling tumor progression. Their expression was not affected in the absence of JunD (figure 3.26).

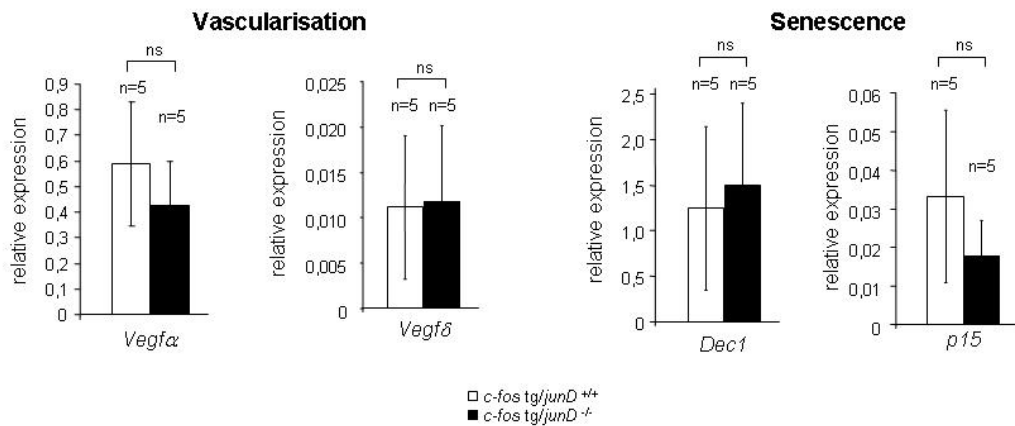


Figure 3.26. mRNA expression of genes related to vascularization (*Vegfa* and *Vegfd*) and senescence (*Dec1* and *p15*) were not altered between tumors from *c-fos tg/junD*^{+/+} and *c-fos tg/junD*^{-/-} mice

3. 6. 3. Expression analysis of genes related to chondrocytes, osteoblasts and osteocytes

Because of the reduced mineral density observed in the tumors from *c-fos tg/junD* KO mice, I checked different marker genes of cell types responsible for the bone formation process. Chondrocyte marker matrix Gla protein (*m-glap*) and Collagen X were expressed at similar levels in tumor samples from *c-fos tg/junD*^{-/-} and *c-fos tg*. Expression of osteoblast marker Runx2 and Collagen I, the most abundant protein in bone were elevated in *c-fos tg/junD*^{-/-} tumor samples in comparison to *c-fos tg* samples albeit this changes were not statistically significant. Sclerostin (*sost*) and Phex which are markers for mature osteocytes were not differentially expressed. One gene that I found down-regulated in a genomic screen (data not shown) was secreted frizzled related protein1 (*sfrp1*). SFRP1 was reported to be a negative regulator of bone formation (Bodine et al., 2004). I also measured the expression of

this gene by quantitative RT-PCR and found it to be down regulated in the *c-fos tg/junD^{-/-}* samples.

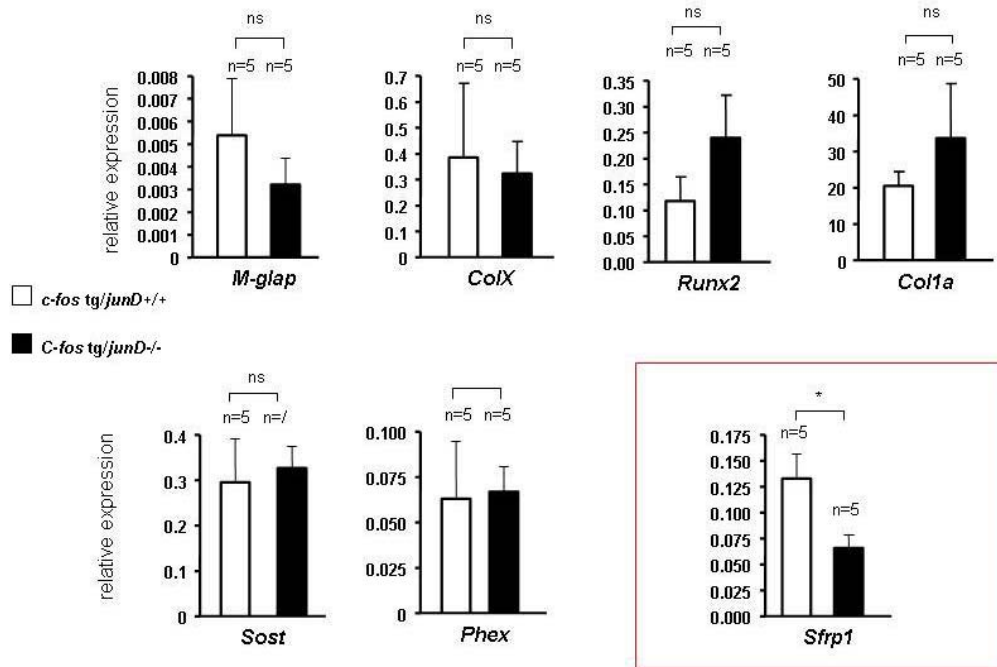


Figure 3.27. mRNA expression of genes related to chondrocytes, osteoblasts and osteocytes. None of the markers were significantly changed except *Sfrp1* which was down-regulated in *c-fos tg/junD^{-/-}* tumours.

The expression data suggest that the process of endochondral bone formation is not disturbed in tumors lacking JunD. In addition, the down regulation of bone formation inhibitor *sfrp1* seemed paradox in light of the reduced bone mass observed in *junD* lacking tumors. Therefore other processes involved in bone remodeling must account for the lower mineralized volume in tumor tissue such as bone resorption. Consequently I analyzed the level of expression of osteoclast related markers.

3. 6. 4. Expression analysis of genes related to osteoclasts

The expression level of the two essential osteoclastogenic factors M-CSF and RANKL were not significantly different in *c-fos tg/junD^{-/-}* and *c-fos tg* tumor samples (figure 3.28). The expression of the receptors to which these factors bind namely RANK and *c-fms*, where not significantly increased. Expression of the decoy receptor

OPG which is a negative regulator for osteoclastogenesis was reduced in *junD* lacking tumors albeit not significantly. Cathepsin K which is a protease important for degradation of collagen specifically expressed by osteoclasts was not changed. However the osteoclast marker TRAP and the coupling molecule Traf6 as well as the c-Fos downstream target NFATc1 essential for osteoclast differentiation were all significantly up-regulated in *c-fos tg|junD^{-/-}* samples. These results were indicative of an increased osteoclastogenesis the *junD* deficient tumour samples.

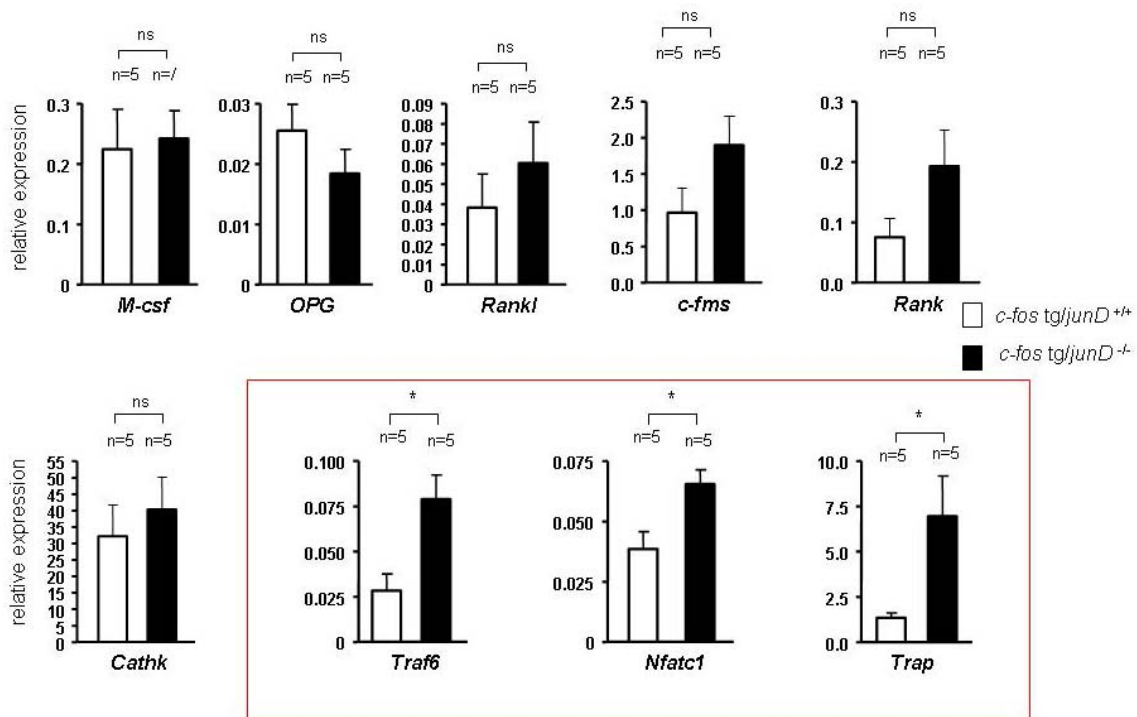


Figure 3.28. Expression of osteoclast markers *Traf6*, *Nfatc1* and *TRAP* was found significantly up-regulated in *c-fos tg|junD^{-/-}* tumour samples indicating increased osteoclastogenesis.

To check for the veracity of if this assumption, I prepared sections from the tumors and stained them for the osteoclast marker TRAP. The number of TRAP-positive cells was increased in *c-fos tg|junD^{-/-}* samples confirming the increase in osteoclast differentiation.

The data suggest that the higher number of osteoclasts could account for an increased resorptive activity in *c-fos tg|junD^{-/-}* tumors that would result in lower mineral content of the tumor.

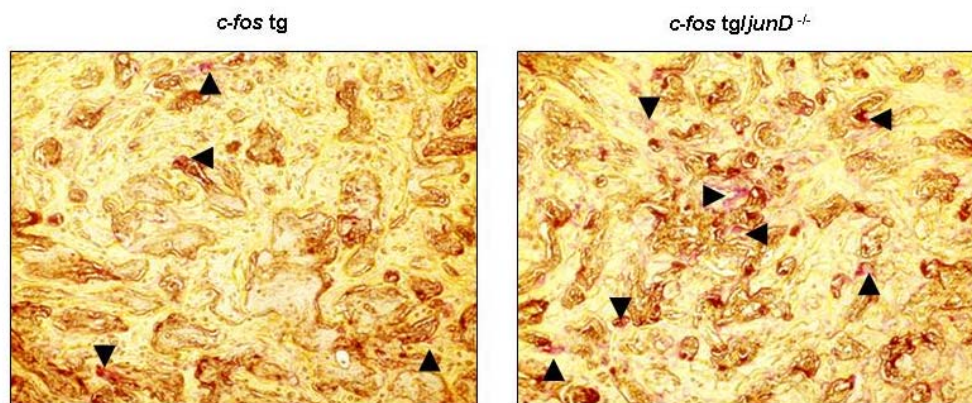


Figure 3.29. Increased number of osteoclasts in *c-fos tg/junD^{-/-}* tumors. TRAP staining of histological section of tumors. TRAP positive cells (in red) are indicated by arrowheads.

3. 7. Expression analysis of osteoblast, osteoclast markers and p27 in calvaria samples from *junD^{-/-}* mice

Because of the observation that on the one hand the lack of JunD leads to increased bone mineral density and on the other hand in combination of elevated c-Fos levels as present in tumors, result in lower bone mineral density, I compared the expression level of osteoclast markers in single mutant *junD* knock out calvarias and wild type controls. The expression levels of *Trap*, *Traf6* and *Nfatc1* were not altered in the calvaria samples of single mutant indicative for no change in osteoclast activity (figure 3.30).

I next measured the expression of *p27* and *sfrp1* in *junD* deficient bone. While *p27* is not altered, *sfrp1* is down-regulated in the *junD* knock out samples (figure 3.30). Therefore JunD-mediated *p27* expression is requiring c-Fos and *sfrp1* expression is not dependant on c-Fos.

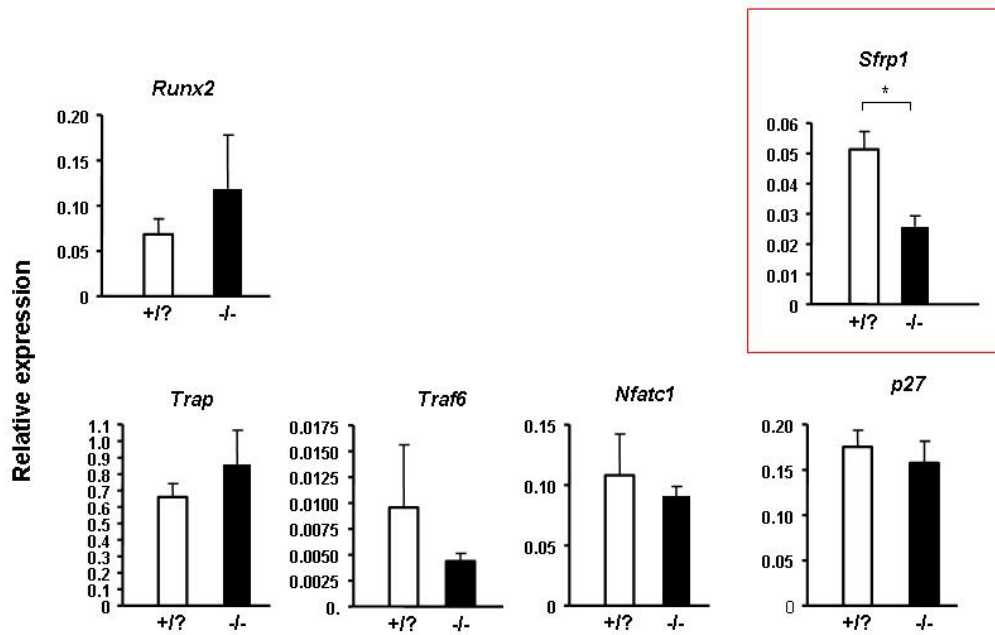


Figure 3.30. Expression of osteoblast, osteoclast marker and *p27* in *junD*^{-/-} single mutant calvaria and control. Osteoclast marker, Runx2 and p27 were not significantly changed. sFRP1 was significantly down-regulated in *junD*^{-/-} calvaria compared to control. +/? means that +/+ and +/- calvaria samples were pooled.